Journal of Molecular Graphics and Modelling 39 (2013) 65–70

Contents lists available at SciVerse ScienceDirect

Journal of Molecular Graphics and Modelling

journal homepage: www.elsevier.com/locate/JMGM

Homology modeling and virtual screening approaches to identify potent inhibitors of slingshot phosphatase 1

Hwangseo Park[a,*], So Ya Park[b], Seong Eon Ryu[b,**]

[a] Department of Bioscience and Biotechnology, Sejong University, 98 Kunja-Dong, Kwangjin-Ku, Seoul 143-747, South Korea
[b] Department of Bioengineering, Hanyang University, 17 Haengdang-dong, Seongdong-gu, Seoul 133-791, South Korea

ARTICLE INFO

Article history:
Accepted 30 October 2012
Available online 8 November 2012

Keywords:
Homology modeling
Virtual screening
Slingshot phosphatase 1
Docking
Inhibitor

ABSTRACT

Although slingshot phosphatase 1 (SSH1) proved to be a promising target for the development of therapeutics for the treatment of vascular diseases and cancers, no small-molecule inhibitor has been reported so far. We have been able to identify eight novel inhibitors of SSH1 through the computer-aided drug design protocol involving homology modeling of SSH1 structure, virtual screening of a large chemical library with docking simulations, and *in vitro* enzyme assays. The identified inhibitors revealed high potencies with the associated IC_{50} values ranging from 2.8 to 12.7 μM and were also screened for having desirable physicochemical properties as a drug candidate. Therefore, they deserve consideration for further development by structure–activity relationship studies to optimize the inhibitory activities. Structural features relevant to the stabilization of the inhibitors in the active site of SSH1 are discussed in detail.

1. Introduction

Dual specificity protein tyrosine phosphatases (DUSPs) are involved in controlling various cellular processes including growth, differentiation, transcription, and metabolism by catalyzing the hydrolysis reaction of phosphorylated protein substrates [1]. DUSP subfamily includes slingshot phosphatases (SSHs) that serve as a specific activator with respect to cofilin [2–4], which is an actin depolymerizing factor and plays the role of controlling the migration of vascular smooth muscle cells [5]. Three isoforms of SSH (SSH1, SSH2, and SSH3) have been identified so far, and they are known to dephosphorylate the phospho-serine group of cofilin at residue 3 [6]. Because cell migration is associated with the pathological remodeling at the region of vascular injury as well as with the invasive capacity of cancer cells, the high activity of SSHs can lead to various vascular diseases and cancer metastasis. In this regard, a series of experimental evidence showed that the down-regulation of SSH1 by small interfering RNA (siRNA) resulted in the decrease of vascular cell migration and the suppression of cancer metastasis [7,8]. Therefore, the control of SSH1 activity by small-molecule inhibitors can be a promising therapeutic strategy for both vascular diseases and cancers.

Although three dimensional (3D) structure of SSH1 has not been known yet, the X-ray crystal structure of its highly homologues protein (SSH2) was reported in complex with a substrate analog [9]. To accommodate the small phosphoserine group in the substrate, SSH2 was found to have a planar and shallow active site in which the negatively charged substrate group could be stabilized by the hydrogen bonds with the backbone amide groups and the side-chain guanidinium ion of the Arg residue located near the catalytic cysteine residue (Cys392). The presence of structural information about the nature of the active site and the interactions with a small-molecule ligand can make it a plausible task to design the potent inhibitors that may develop into a drug candidate. Indeed, the usefulness of such structural information has been well appreciated in designing the potent and selective small-molecule inhibitors of various phosphatases [10,11]. Nonetheless, the discovery of SSH inhibitors has lagged behind the biochemical and structural studies. To the best of our knowledge, no small-molecule SSH inhibitor has been reported so far in the literature.

In the present study, we aim to identify the potent SSH1 inhibitors by means of a structure-based drug design protocol involving homology modeling, virtual screening with docking simulations, and *in vitro* enzyme assay. The characteristic feature that discriminates our virtual screening approach from the others lies in the implementation of an accurate solvation model in calculating the binding free energy between SSH1 and the putative ligands, which would have an effect of increasing the hit rate in enzyme assay [12]. We find in this study that the docking simulations with the improved binding free energy function can be a useful

* Corresponding author. Tel.: +82 2 3408 3766; fax: +82 2 3408 4334.
** Corresponding author. Tel.: +82 2 2220 2349; fax: +82 2 2220 4023.
E-mail addresses: hspark@sejong.ac.kr (H. Park), ryuse@hanyang.ac.kr (S.E. Ryu).

1093-3263/$ – see front matter © 2012 Elsevier Inc. All rights reserved.
http://dx.doi.org/10.1016/j.jmgm.2012.10.008

computational tool for elucidating the activities of the identified inhibitors, as well as for enriching the chemical library with molecules that are likely to have desired biological activities.

2. Methods

Because 3D structure of SSH1 has not been reported so far, we carried out the homology modeling using the X-ray crystal structure of SSH2 (PDB entry: 2NT2) [9] as the template to generate the structure of SSH1 suitable for the virtual screening with docking simulations. Sequence alignment between the phosphatase domains of SSH2 and SSH1 was derived with the ClustalW program [13] using the BLOSUM matrices for scoring the alignments. The parameters of GAP OPEN, GAP EXTENTION, and GAP DISTANCE were set equal to 10, 0.05, 8, respectively. Opening and extension gap penalties were thus changed systematically, and the obtained alignment was inspected for violation of structural integrity in the structurally conserved regions. On the basis of the best-scored sequence alignment, 3D structure of the catalytic domain of SSH1 was constructed using the latest version of the MODELLER program [14]. In this model building, we employed an optimization method involving conjugate gradients and molecular dynamics to minimize the violations of the spatial restraints. With respect to the structure of gap regions, the coordinates were built from a randomized distorted structure that resides approximately between the two anchoring regions as implemented in the MODELLER program. To increase the accuracy of the calculated structures, loop modeling was also performed with the enumeration algorithm [15]. Then we calculated the conformational energies of the predicted SSH1 structure with ProSa 2003 program [16] for the purpose of evaluation.

The atomic coordinates of SSH1 obtained from the homology modeling were used as the receptor model in the virtual screening with docking simulations. Special attention was paid to the assignment of the protonation states of the ionizable Asp, Glu, His, and Lys residues in the homology-modeled structure of SSH1. The Asp and Glu side chains were assumed to be neutral if one of their carboxylate oxygens pointed toward a hydrogen-bond accepting group including the backbone aminocarbonyl oxygen at a distance within 3.5 Å, which is generally accepted as the distance limit for a hydrogen bond of moderate strength [17]. Similarly, the lysine side chains were assumed to be protonated unless an NZ atom was proximal to a hydrogen-bond donating group. The same procedure was applied toward determining the protonation states of the ND and NE atoms in the His residues. After determining the protonation state of each protein atom, we carried out 200 cycles of energy minimization with the AMBER program to remove the bad steric contacts.

The docking library for SSH1 comprising about 240,000 compounds was constructed from the latest version of the chemical database distributed by Interbioscreen (http://www.ibscreen.com) containing approximately 477,000 synthetic and natural compounds. Prior to the virtual screening with docking simulations, they were filtrated on the basis of Lipinski's "Rule of Five" to adopt only the compounds with the physicochemical properties of potential drug candidates [18] and without reactive functional group(s). To remove the structural redundancies in the chemical library, the structurally similar compounds with Tanimoto coefficient larger than 0.8 were clustered into a single representative molecule. As a consequence, a docking library consisting of ~240,000 compounds was constructed. These pre-filtrated compounds were then processed with the CORINA program to generate their 3D atomic coordinates, followed by the assignment of Gasteiger–Marsili atomic charges [19]. We used the AutoDock program [20] in the virtual screening of SSH1 inhibitors because the outperformance of its scoring function over those of the others had been shown in several target proteins [21]. AMBER force field parameters were assigned for calculating the van der Waals interactions and the internal energy of a ligand as implemented in the original AutoDock program. Docking simulations with AutoDock were then carried out in the active site of SSH1 to score and rank the compounds in the docking library according to their calculated binding affinities.

In the actual docking simulation of the compounds in the docking library, we used the empirical AutoDock scoring function improved by the implementation of a new solvation free energy function for organic molecules. The modified scoring function has the following form.

$$\begin{aligned}\Delta G^{\mathrm{aq}}_{\mathrm{bind}} = {} & W_{\mathrm{vdW}} \sum_{i=1} \sum_{j=1} \left(\frac{A_{ij}}{r_{ij}^{12}} - \frac{B_{ij}}{r_{ij}^{6}} \right) \\ & + W_{\mathrm{hbond}} \sum_{i=1} \sum_{j=1} E(t) \left(\frac{C_{ij}}{r_{ij}^{12}} - \frac{D_{ij}}{r_{ij}^{10}} \right) \\ & + W_{\mathrm{elec}} \sum_{i=1} \sum_{j=1} \frac{q_i q_j}{\varepsilon(r_{ij}) r_{ij}} \\ & + W_{\mathrm{tor}} N_{\mathrm{tor}} + W_{\mathrm{sol}} \sum_{i=1} S_i \left(O_i^{\max} - \sum_{j \neq i} V_j e^{-r_{ij}^2/2\sigma^2} \right) \end{aligned} \quad (1)$$

where W_{vdW}, W_{hbond}, W_{elec}, W_{tor}, and W_{sol} are the weighting factors of van der Waals, hydrogen bond, electrostatic interactions, torsional term, and desolvation cost for the binding of an inhibitor in the active site, respectively. r_{ij} represents the interatomic distance, and A_{ij}, B_{ij}, C_{ij}, and D_{ij} are related to the depths of the potential energy well and the equilibrium separations between the two atoms. The hydrogen bond term has an additional weighting factor, $E(t)$, representing the angle-dependent directionality. Cubic equation approach was applied to obtain the dielectric constant required in computing the interatomic electrostatic interactions between SSH1 and a ligand molecule [22]. In the entropic term, N_{tor} is the number of rotatable bonds in the ligand. In the desolvation term, S_i and V_i are the solvation parameter and the fragmental volume of atom i [23], respectively, while $O_i{}^{\max}$ stands for the maximum atomic occupancy. In the calculation of molecular solvation free energy term in Eq. (1), we used the atomic parameters developed by Kang et al. [24] because those of the atoms other than carbon were unavailable in the current version of AutoDock. This modification of the solvation free energy term is expected to increase the accuracy in virtual screening because the underestimation of ligand solvation often leads to the overestimation of the binding affinity of a ligand with many polar atoms [12]. Indeed, the superiority of this modified scoring function to the previous one was well-appreciated in recent studies for virtual screening of kinase and phosphatase inhibitors [25,26].

The gene for the phosphatase domain of SSH1 corresponding to residues 305–461 (SSH1-cat) was cloned into the *E. coli* expression vector pET28a. Cells containing the vector were induced with 0.2 mM IPTG and grown further at 18 °C for 16 h. Cell pellets were resuspended in the lysis buffer containing 50 mM Tris–HCl (pH 7.5), 0.5 M NaCl, 1% PMSF, and 5% glycerol. The resuspension was then lysed by sonication on ice. The His-tagged SSH1-cat was purified by Ni-NTA agarose column and dialyzed against 20 mM Tris–HCl (pH 8.0), 5 mM EDTA, 50 mM NaCl, and 5% glycerol. Total 148 compounds selected from the virtual screening were evaluated for *in vitro* inhibitory activity against the purified SSH1-cat. These enzyme assays were performed by monitoring the extent of hydrolysis of 6,8-difluoro-4-methyl-umbelliferyl phosphate (DiFMUP) with a spectrofluorometric assay. Although many PTPs were most active around pH 6, SSH1 revealed the highest enzymatic activity

Fig. 1. Sequence alignment of the phosphatase domains of SSH1 and SSH2.

in buffer solutions with pH 8.0 as in the case of mitogen-activated protein kinase phosphatase-1 (MKP1) [26]. At the enzyme concentration of 100 nM, we determined the concentration of DiFMUP at which the enzymatic reaction system could exhibit a typical Michaelis–Menten kinetics. When the substrate concentration increased to 10 μM, the amount of product increased gradually and converged to the maximum with the elapse of reaction time. Therefore, the enzyme assays were performed at DiFMUP concentration of 10 μM. The purified SSH1-cat (100 nM), DiFMUP (10 μM), and a candidate inhibitor were incubated in the reaction mixture containing 20 mM Tris–HCl (pH 8.0), 0.01% Trition X-100, and 5 mM DTT for 20 min. The resulting fluorescence was measured at 460 nm by using the Perkin Elmer 2030 instrument.

As a check for the presence of impurities, the purities of the compounds that inhibited the catalytic activity of SSH1 by more than 50% at the concentration of 20 μM were determined with high performance liquid chromatography (HPLC) using Shimadzu HPLC Prominence system with 4.6 mm × 150 mm HPLC column at the wavelengths of 254 and 280 nm. We used the two-mobile phase system comprising 0.1% TFA-water (A) and 100% acetonitrile (B) for a reversed-phase gradient elution. Elutions were then performed with the flow rate of 1.3 mL/min from 30% of B to 70% of B in 20 min, then back to 30% of B in 10 min. The purities the eight putative inhibitors were determined to be 95.4, 96.6, 97.1, 93.8, 94.5, 98.3, 96.1, and 95.2%. Judging from these high purities, the inhibitory activities of the identified inhibitors seem to stem from their direct interactions with SSH1 instead of the unwanted interactions between SSH1 and impurities.

The inhibitory activities of the putative SSH1 inhibitors were measured in duplicate at the concentrations of 0.0, 0.1, 0.5, 1.0, 2.0, 5.0, 10, 20, and 50 μM to obtain the dose–response curve fits. The IC_{50} value of each inhibitor was then determined from direct regression analysis using the four-parameter sigmoidal curve as implemented in the SigmaPlot program.

3. Results and discussion

The peptide sequence of human SSH1 comprising 1049 amino acid residues was retrieved from UniProtKB protein knowledgebase (http://www.uniprot.org, accession number: Q8WYL5). Domain analysis of the whole amino acid sequence indicated that residues 308–448 would correspond to the protein tyrosine phosphatase domain with the catalytic cysteine residue at position 393. Although 3D structure of the phosphatase domain of SSH1 has not been reported so far, SSH2 was found to be highly homologous to SSH1 in the database search at NCBI BLAST (http://blast.ncbi.nlm.nih.gov). As can be seen in Fig. 1, the identity and similarity between the amino acid sequences of the phosphatase domains of SSH2 and SSH1 amount to 74.6% and 90.1%, respectively. Such a high sequence identity between the template (SSH2) and the target (SSH1) indicates that a high-quality structure of SSH1 can be generated in the homology modeling [27]. To obtain the 3D structure required for virtual screening of SSH1 inhibitors, therefore, we constructed the structural model for the phosphatase domain of SSH1 through the homology modeling using the X-ray crystal structure of SSH2 as the template.

The structural model for the phosphatase domain of SSH1 obtained from the homology modeling was evaluated with the ProSa 2003 program [16] by examining whether the interactions of each residue with the rest of the protein structure could be maintained favorable. This program calculates the knowledge-based mean fields to judge the quality of protein folds and has been widely used to estimate the stability of a protein conformation. Fig. 2 compares the ProSa 2003 energy profiles of the homology-modeled structure of SSH1 and the X-ray crystal structure of SSH2. We note that the ProSa energy remains negative for each amino acid residue in both cases, indicating that both protein structures should be physically acceptable. More interestingly, the stability of the homology-modeled SSH1 structure appears to be comparable to that of the X-ray structure of SSH2 in most protein regions except for N- and C-terminal regions, which supports the accuracy of the predicted SSH1 structure.

Of the 240,000 compounds screened with docking simulations in the active site of the homology-modeled SSH1 structure, 150 top-scored compounds were selected as virtual hits. 148 of them were available from the compound supplier and tested for inhibitory activity against SSH1 by *in vitro* enzyme assay. As a result, we identified eight compounds that inhibited the catalytic activity of SSH1 by more than 50% at the concentration of 20 μM, which were selected to determine the IC_{50} values. The chemical structures and the inhibitory activities of the newly identified inhibitors are shown in Fig. 3 and Table 1, respectively. Also, the dose–response behaviors of the inhibitors measured to obtain their IC_{50} values are shown in Fig. 4. We note that compounds **1**–**8** exhibit high inhibitory activities with the associated IC_{50} values ranging from 2.8 to 12.7 μM. These inhibitors seem to be capable of establishing strong multiple hydrogen bonds in the active site of SSH1. Benzoate, benzene-1,2-diol, 5-imino-5,6-dihydro-[1,3,4]thiadiazolo[3,2-*a*]pyrimidin-7-one, and [1,2,4]triazolo[3,4-*b*][1,3,4]thiadiazole moieties included in molecular structures of

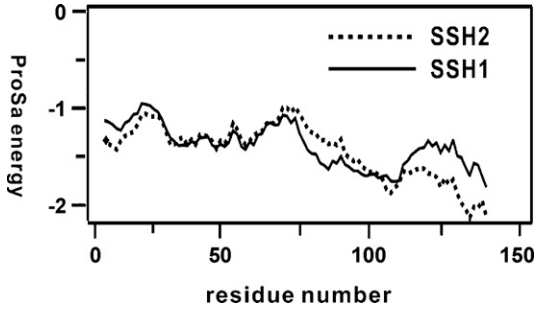

Fig. 2. Comparative view of the ProSa 2003 energy profiles for the X-ray structure of SSH2 and the homology-modeled SSH1 structure. For convenience, the amino acids are renumbered from 1 instead of retaining the original numbers.

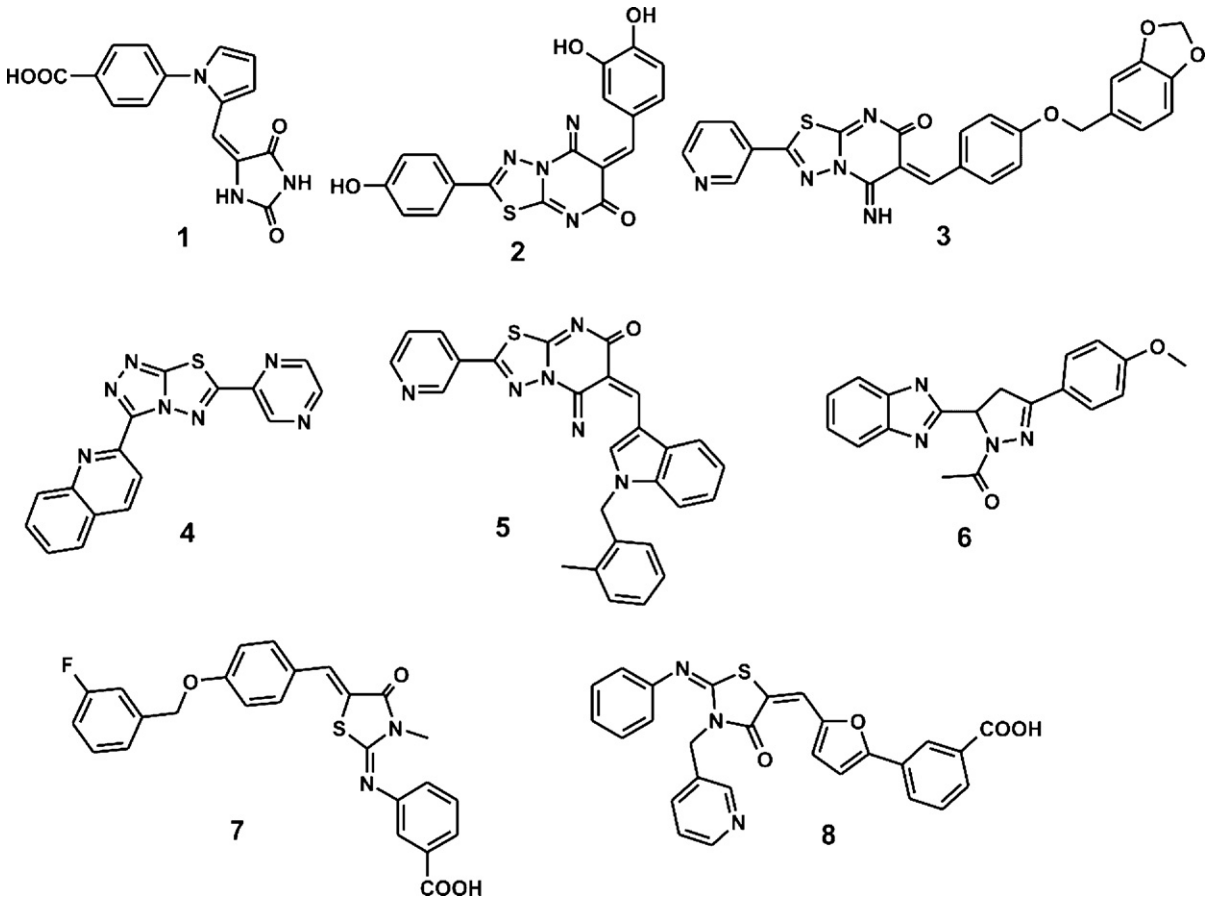

Fig. 3. Chemical structures of the eight SSH1 inhibitors identified in this study.

1–**8** are expected to serve as a surrogate for the phosphoserine group of the cofilin substrate. Although **1** was also known as an inhibitor of the phosphatase of regenerating liver 3 (PRL-3), none of the compounds **2**–**8** has been reported as a phosphatase inhibitor so far. Furthermore, no additional biological activity was found at least in the two most public chemical databases, ChEMBL and PubChem. Therefore, they deserve consideration for further development by structure–activity relationship (SAR) studies to develop therapeutics for vascular diseases and cancers.

Because the selectivity has been one of the most important issues in the development of phosphatase inhibitors, we compared the inhibitory activities of **1**–**8** for SSH1 to those for two other phosphatases, SSH2 and PRL-3. As can be seen in Table 1, all of the SSH1 inhibitors found in this study reveal lower potencies for SSH2 and PRL-3 than for SSH1 although **2** and **3** appear to be also an effective inhibitor of SSH2 and PRL-3. In particular, **1** and **4**–**8** are found to be almost inactive against PRL-3. Thus, the inhibitors **1**–**8** seem to be more potent for SSH1 than for the other structurally similar phosphatases. The selectivities of the identified inhibitors also indicate that they would impair the enzymatic activity of SSH1 through the non-bond interactions in the active site instead of making a covalent bond with the side-chain thiolate ion of the catalytic cysteine residue contained in most of DUSPs in common.

Table 1
IC_{50} values (in μM) of **1**–**8** with respect to SSH1, SSH2, and PRL-3.

Compounds	SSH1	SSH2	PRL-3
1	2.8	28.7	>100
2	3.1	7.4	33.2
3	4.1	22.4	27.6
4	5.0	16.2	>100
5	7.2	27.0	>100
6	10.8	20.6	>100
7	11.4	78.6	>100
8	12.7	39.6	>100

In order to get structural insight into the inhibitory mechanisms of the identified SSH1 inhibitors, we investigated their binding modes in the active in a comparative fashion. Fig. 5 shows the lowest-energy conformations of **1**–**8** in active site gorge of SSH1 calculated with the modified AutoDock program. The results of these docking simulations are self-consistent in the sense that the functional groups of similar chemical character are placed in similar ways with comparable interactions with the protein groups. As revealed by the superposition of the docked structures, for example, the hydrophilic moieties that serve as a surrogate for the substrate phosphoserine group are directed to the PTP loop including the catalytic cysteine residue (Cys393) while the hydrophobic groups point toward WPD loop and the loop connecting the two alpha helices (α5 and α6). These common features in the calculated binding modes indicate that a potent SSH1 inhibitor should include an effective surrogate for the substrate phosphoserine group and simultaneously the hydrophobic groups for binding to the loop structures near the active site. To examine the possibility of the allosteric inhibition of SSH1 by the identified inhibitors, docking simulations were carried out with the grid maps for the receptor model so as to include the entire phosphatase domain of SSH1. However, the binding configuration in which an inhibitor resides outside the active site was not observed for any of the inhibitors found in this study. These results support the possibility that the

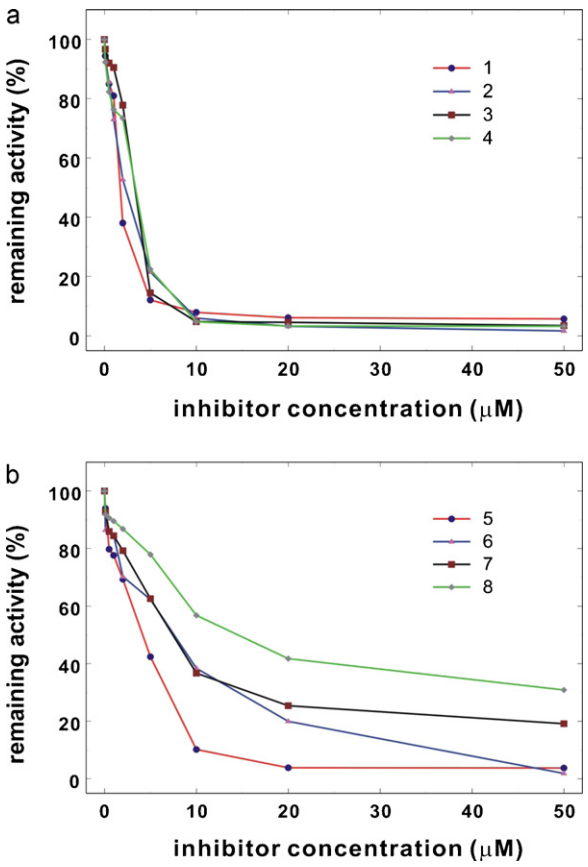

Fig. 4. Dose–response curves of (a) **1**, **2**, **3**, and **4**, and (b) **5**, **6**, **7**, and **8** for the inhibition of SSH1.

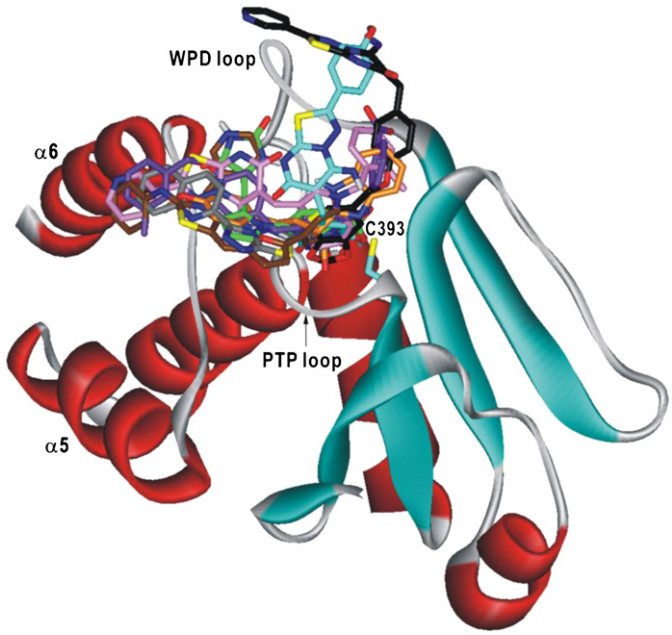

Fig. 5. Comparative view of the binding modes of **1**–**8** in the active site of SSH1. Carbon atoms of **1**–**8** are indicated in green, cyan, black, gray, pink, orange, violet, and brown, respectively. The positions of α5, α6, PTP loop, WPD loop, and Cys393 are also indicated.

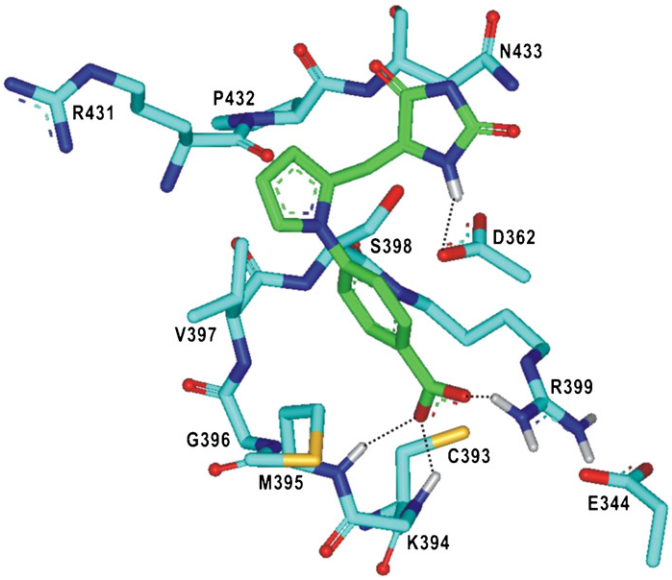

Fig. 6. Calculated binding mode of **1** in the active site of SSH1. Each dotted line indicates a hydrogen bond.

inhibitors would impair the catalytic activity of SSH1 through the binding in the active site.

The calculated binding mode of **1** in the active site of SSH1 is illustrated in Fig. 6. We note that one of the terminal carboxylate oxygens of **1** receives two hydrogen bonds from the backbone amidic groups of Lys394 and Met395 in a bifurcated form at the bottom of active site. The other carboxylate oxygen appears to form a hydrogen bond with the side chain guanidinium ion of Arg399. Apparently, these three hydrogen bonds involving the carboxylate ion should serve as an anchor for positioning the inhibitor at the active site. It is also noted that the carboxylate carbon of **1** resides in the vicinity of the side-chain thiolate group of Cys393 with the associated interatomic distance of 3.61 Å. Judging from the proximity to Cys393 and the formation of multiple hydrogen bonds in the active site, the benzoate moiety of **1** seems to be an effective surrogate for the phosphoserine group in cofilin substrate. An additional hydrogen bond is observed between one of the amidic nitrogens on imidazolidine-2,4-dione ring of **1** and the side-chain carboxylate ion of Asp362, which should also be a significant binding force in the SSH1-**1** complex. The inhibitor **1** can be further stabilized in the active site of SSH1 by the hydrophobic interactions of its nonpolor groups with the side chains of Met395, Val397, and Pro432. Thus, the overall structural features in the calculated SSH1-**1** complex indicate that the micromolar inhibitory activity of **1** should stem from the multiple hydrogen bonds and hydrophobic interactions established simultaneously in the active site. **1** is expected to serve as a good inhibitor scaffold from which much more potent inhibitors can be derivatized because of its low molecular weight of ~297.

Fig. 7 shows the lowest-energy binding mode of **2** in the active site of SSH1. The binding mode of **2** is similar to that of **1** in that the roles of hydrogen bond donor with respect to the terminal benzene-1,2-diol moiety of **2** are played by the side-chain guanidinium ion of Arg399 and the backbone amidic groups located at the bottom of the active site. One of the terminal —OH moieties of **2** appears to stabilize the side-chain thiolate ion of Cys393 by donating a hydrogen bond. These structural features of the hydrogen-bond interactions indicate that the benzene-1,2-diol group of **2** can also serve as an effective surrogate for the phosphoserine group in the substrate of SSH1. A stable hydrogen bond is also established

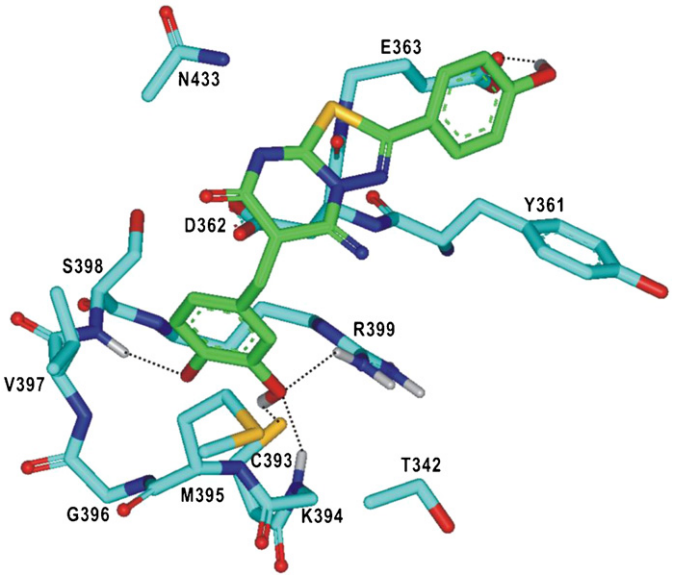

Fig. 7. Calculated binding mode of **2** in the active site of SSH1. Each dotted line indicates a hydrogen bond.

between the terminal phenolic moiety of **2** and side-chain carboxylate ion of Glu363, which should play a significant role in stabilizing the inhibitor in the active site. Hydrophobic interactions in the SSH1-**2** complex are found to be established also in a similar fashion to those in the SSH1-**1** complex: the nonpolar groups of **2** form the van der Waals contacts with the side chains of Tyr361, Met395, and Val397. The similarities in structural features of both hydrogen-bond and van der Waals interactions in SSH1-**1** and SSH1-**2** complexes can thus be invoked to explain the similar inhibitory activities of **1** and **2** (Table 1).

4. Conclusions

We have identified eight novel inhibitors of SSH1 by applying a computer-aided drug design protocol involving the homology modeling and the structure-based virtual screening with docking simulations under consideration of the effects of ligand solvation in the scoring function. These inhibitors reveal a high potency with IC_{50} values ranging from 2.8 to 12.7 μM and have desirable physicochemical properties as a drug candidate. Therefore, each of the newly discovered inhibitors deserves consideration for further development by SAR studies to develop therapeutics for vascular diseases and cancers. Detailed binding mode analyses with docking simulations indicate that the inhibitors can be stabilized in active site by the simultaneous establishment of multiple hydrogen bonds and van der Waals contacts.

Acknowledgments

This work was supported by Basic Science Research Program through the National Research Foundation of Korea (NRF) funded by the Ministry of Education, Science and Technology (2012-0008440), and a Hanyang University internal grant.

References

[1] A. Farooq, M.M. Zhou, Structure and regulation of MAPK phosphatases, Cellular Signalling 16 (2004) 769–779.
[2] R.A. Gungabissoon, J.R. Bamburg, Regulation of growth cone actin dynamics by ADF/cofilin, Journal of Histochemistry and Cytochemistry 51 (2003) 411–420.
[3] M. Van Troys, L. Huyck, S. Leyman, S. Dhaese, J. Vandekerkhove, C. Ampe, Ins and outs of ADF/cofilin activity and regulation, European Journal of Cell Biology 87 (2008) 649–667.
[4] K. Kligys, J.N. Claiborne, P.J. DeBiase, S.B. Hopkinson, Y. Wu, K. Mizuno, J.C. Jones, The slingshot family of phosphatases mediates Rac1 regulation of cofilin phosphorylation, laminin-332 organization, and motility behavior of keratinocytes, Journal of Biological Chemistry 282 (2007) 32520–32528.
[5] T.Y. Huang, C. DerMardirossian, G.M. Bokoch, Cofilin phosphatases and regulation of actin dynamics, Current Opinion in Cell Biology 18 (2006) 26–31.
[6] P.D. Sarmiere, J.R. Bamburg, Regulation of the neuronal actin cytoskeleton by ADF/cofilin, Journal of Neurobiology 58 (2004) 103–117.
[7] R.A. Torres, D.A. Drake, V. Solodushko, R. Jadhav, E. Smith, P. Rocic, D.S. Weber, Slingshot isoform-specific regulation of cofilin-mediated vascular smooth muscle cell migration and neointima formation, Arteriosclerosis, Thrombosis, and Vascular Biology 31 (2011) 2424–2431.
[8] Y. Horita, K. Ohashi, M. Mukai, M. Inoue, K. Mizuno, Suppression of the invasive capacity of rat ascites hepatoma cells by knockdown of Slingshot or LIM kinase, Journal of Biological Chemistry 283 (2008) 6013–6021.
[9] S.K. Jung, D.G. Jeong, T.-S. Yoon, J.H. Kim, S.E. Ryu, S.J. Kim, Crystal structure of human slingshot phosphatase 2, Proteins 68 (2007) 408–412.
[10] R. Hayashi, K. Tanoue, S.R. Durell, D.K. Chatterjee, L.M. Jenkins, D.H. Appella, E. Appella, Optimization of a cyclic peptide inhibitor of Ser/Thr phosphatase PPM1D (Wip1), Biochemistry 50 (2011) 4537–4549.
[11] R. Ottanà, R. Maccari, S. Amuso, G. Wolber, D. Schuster, S. Herdlinger, G. Manao, G. Camici, P. Paoli, New 4-[(5-arylidene-2-arylimino-4-oxo-3-thiazolidinyl)methyl]benzoic acids active as protein tyrosine phosphatase inhibitors endowed with insulinomimetic effect on mouse C2C12 skeletal muscle cells, European Journal of Medical Chemistry 50 (2012) 332–343.
[12] B.K. Shoichet, A.R. Leach, I.D. Kuntz, Ligand solvation in molecular docking, Proteins 34 (1999) 4–16.
[13] J.D. Thompson, D.G. Higgins, T.J. Gibson, CLUSTAL W: improving the sensitivity of progressive multiple sequence alignment through sequence weighting, position-specific gap penalties and weight matrix choice, Nucleic Acids Research 22 (1994) 4673–4680.
[14] A. Sali, T.L. Blundell, Comparative protein modelling by satisfaction of spatial restraints, Journal of Molecular Biology 234 (1993) 779–815.
[15] A. Fiser, R.K. Do, A. Sali, Modeling of loops in protein structures, Protein Science 9 (2000) 1753–1773.
[16] M.J. Sippl, Recognition of errors in three-dimensional structures of proteins, Proteins 17 (1993) 355–362.
[17] G.A. Jeffrey, An Introduction to Hydrogen Bonding, Oxford University Press, Oxford, 1997.
[18] C.A. Lipinski, F. Lombardo, B.W. Dominy, P.J. Feeney, Experimental and computational approaches to estimate solubility and permeability in drug discovery and development settings, Advanced Drug Delivery Reviews 23 (1997) 3–20.
[19] J. Gasteiger, M. Marsili, Iterative partial equalization of orbital electronegativity – a rapid access to atomic charges, Tetrahedron 36 (1980) 3219–3228.
[20] G.M. Morris, D.S. Goodsell, R.S. Halliday, R. Huey, W.E. Hart, R.K. Belew, A.J. Olson, Automated docking using a Lamarckian genetic algorithm and an empirical binding free energy function, Journal of Computational Chemistry 19 (1998) 1639–1662.
[21] H. Park, J. Lee, S. Lee, Critical assessment of the automated AutoDock as a new docking tool for virtual screening, Proteins 65 (2006) 549–554.
[22] H. Park, J.H. Jeon, Cubic equation governing the outer-region dielectric constant of globular proteins, Physical Review E 75 (2007) 021916.
[23] P.F.W. Stouten, C. Frömmel, H. Nakamura, C. Sander, An effective solvation term based on atomic occupancies for use in protein simulations, Molecular Simulation 10 (1993) 97–120.
[24] H. Kang, H. Choi, H. Park, Prediction of molecular solvation free energy based on the optimization of atomic solvation parameters with genetic algorithm, Journal of Chemical Information and Modeling 47 (2007) 509–514.
[25] H. Park, O. Chi, J. Kim, S. Hong, Identification of novel inhibitors of tropomyosin-related kinase A through the structure-based virtual screening with homology-modeled protein structure, Journal of Chemical Information and Modeling 51 (2011) 2986–2993.
[26] H. Park, J.Y. Jeon, S.Y. Kim, D.G. Jeong, S.E. Ryu, Identification of novel inhibitors of mitogen-activated protein kinase phosphatase-1 with structure-based virtual screening, Journal of Computer-Aided Molecular Design 25 (2011) 469–475.
[27] D. Baker, A. Sali, Protein structure prediction and structural genomics, Science 294 (2001) 93–96.